Proceedings of the ASME 2016 Dynamic Systems and Control Conference
DSCC2016
October 12-14, 2016, Minneapolis, Minnesota, USA

DSCC 2016-9801

NONLINEAR MODEL PREDICTIVE CONTROL STRATEGIES FOR A PARALLEL EVAPORATOR DIESEL ENGINE WASTE HEAT RECOVERY SYSTEM

Adamu Yebi
Clemson University - International Center for Automotive Research
Greenville, South Carolina, USA

Bin Xu
Clemson University - International Center for Automotive Research
Greenville, South Carolina, USA

Xiaobing Liu
BorgWarner Inc.
Auburn Hills, Michigan, USA

John Shutty
BorgWarner Inc.
Auburn Hills, Michigan, USA

Paul Anschel
BorgWarner Inc.
Auburn Hills, Michigan, USA

Simona Onori
Clemson University - International Center for Automotive Research
Greenville, South Carolina, USA

Zoran Filipi
Clemson University - International Center for Automotive Research
Greenville, South Carolina, USA

Mark Hoffman
Clemson University - International Center for Automotive Research
Greenville, South Carolina, USA

ABSTRACT

This paper discusses the control challenges of a parallel evaporator organic Rankine cycle (ORC) waste heat recovery (WHR) system for a diesel engine. A nonlinear model predictive control (NMPC) is proposed to regulate the mixed working fluid outlet temperature of both evaporators, ensuring efficient and safe ORC system operation. The NMPC is designed using a reduced order control model of the moving boundary heat exchanger system. In the NMPC formulation, the temperature difference between evaporator outlets is penalized so that the mixed temperature can be controlled smoothly without exceeding maximum or minimum working fluid temperature limits in either evaporator. The NMPC performance is demonstrated in simulation over an experimentally validated, high fidelity, physics based ORC plant model. NMPC performance is further validated through comparison with a classical PID control for selected high load and low load engine operating conditions. Compared to PID control, NMPC provides significantly improved performance in terms of control response time, overshoot, and temperature regulation.

I. INTRODUCTION

In the recent years, waste heat recovery (WHR) technology has been explored to meet stringent emission reduction regulations and reduce fuel consumption [1]. WHR technology is particularly applicable to heavy duty vehicles, owing to their utilization with long-haul drive cycles. As a result, a significant volume of research has been aimed at WHR application on heavy duty trucks [2]-[8]. These studies have obtained varying degrees of success: Cummins reported the ORC-WHR system achieved 3.6% absolute brake thermal efficiency (BTE) improvement for the on-road tractor-trailer fleet by using both EGR and exhaust gas streams as heat sources [2]. Daimler achieved 2% absolute BTE improvement for on-road tractor-trailer fleet using exhaust gas, radiator and charge air as heat sources [2]. Based on a 12 L heavy duty diesel engine, Bosch experimentally obtained 2.1kW, 5.3kW and 9.0kW turbine generated power from B25, B50, and B75 engine operating conditions, respectively [8].

Among the existing WHR technologies, ORC has become the most popular in the heavy duty sector due to its relative cost effectiveness and ease of adaptability for low temperature heat sources [9-12]. Current ORC systems recover energy from engine exhaust in the form of mechanical power, which can be either transferred to the engine drivetrain directly or converted to electricity through an electric generator. However, efficient and safe operation of ORC system is limited by the highly transient nature of the heat source (engine exhaust), which depends on driving conditions. Optimal operation is only possible in a very narrow range of working fluid evaporating pressure and temperature. The maximum applicable operating temperature is constrained by dissociation and degradation of the working fluid while the lower constraint is fixed by condensation of working

fluid in the expansion device. Thus, a precise control system design is crucial for optimal ORC system operation.

Some work has addressed the ORC system control challenge [13-19]. Most of the published control design works are dedicated to single evaporator based ORC systems [13, 14, 16-19], while little has been published on ORC control for parallel evaporator designs [15]. Single evaporator based ORC systems are typically utilize tail pipe (TP) exhaust gas as the sole heat source. For parallel evaporator designs, exhaust gases from the tail pipe and exhaust gas recirculation (EGR) loop are commonly utilized to maximize the energy recovered from engine exhaust.

Parallel boiler ORC systems pose additional control design challenges because it requires a coordinated effort to split flow through each evaporators. The primary actuator for evaporator outlet temperature control is the working fluid pump speed, which adjusts the working fluid mass flow rate. For parallel boiler configurations which utilize a single pump, coordinated actuation of both evaporators for mixed evaporator outlet working fluid temperature control is not trivial. In [15], separate actuators (bypass valves) are considered for each evaporator which independently return working fluid to the reservoir. This ORC system is relatively simple to control compared to one actuated by only single pump, which is the case considered in the current paper.

In addition to the need for coordinated actuation, coupling of strongly nonlinear system dynamics and the distinctly different time constants of two parallel evaporators (TP/EGR) make control of the mixed working fluid evaporator outlet temperature a difficult problem. In this regard, a conventional control approach like PID may not provide satisfactory performance over a wide range of engine operating conditions. For such a challenging control problem, model predictive control (MPC) is a potential candidate since it handles multivariable problems naturally and can reject any measurable disturbance ahead of time. A linear MPC based on a switching linear model has been proven applicable for ORC control over highly transient engine operating conditions [15].

In this paper, we consider a nonlinear model predictive control (NMPC) based on a reduced order nonlinear moving boundary heat exchanger model to regulate the mixed evaporator outlet temperature. In the NMPC formulation, three different control strategies for splitting the working fluid mass flow through the parallel evaporators are considered. The NMPC formulation is limited to the evaporator temperature control, where satisfactory performance is difficult to obtain with conventional approaches. For evaporator outlet pressure control, one can consider a separate PID loop to reduce the computation burden of NMPC. Due to faster dynamics of the pressure, its control is decoupled from temperature control. The effectiveness of the proposed control scheme is illustrated over an experimentally validated, high fidelity, physics-based ORC plant model.

The remainder of the paper is organized as follows. Section II presents the system description of parallel evaporator ORC system. Section III presents the heat exchanger models including both the finite volume model (FVM) of the physics based plant model and the reduced order control model or moving boundary model (MBM). Section IV discusses the NMPC problem formulation including the control strategy for coordinated actuation of both boilers (TP/EGR). Section V provides demonstrative simulation results and discussions. Conclusions are then presented in Section VI.

NOMENCLATURE

A Area $[m^2]$
ρ Density $[kg/m^3]$
$\dot{m}$ Mass flow rate $[kg/s]$
z Spatial position in axial direction $[m]$
h Enthalpy $[J/kg]$
p Pressure $[Pa]$
D Diameter $[m]$
U Heat transfer coefficient $[J/(m^2 \cdot K)]$
c_p Isobaric specific heat capacity $[J/(kg \cdot K)]$
V Volume $[m^3]$
T Temperature [K]

II. SYSTEM DESCREPTION

The ORC system schematic is shown in Fig. 1. The main components include: a high pressure pump, tail pipe and EGR evaporators, a turbine expander and a condenser. The system also contains auxiliary components such as an expansion tank after the condenser, a low pressure feed pump before the high pressure pump, two working fluid mass flow distribution valves, a turbine inlet valve and a turbine bypass valve.

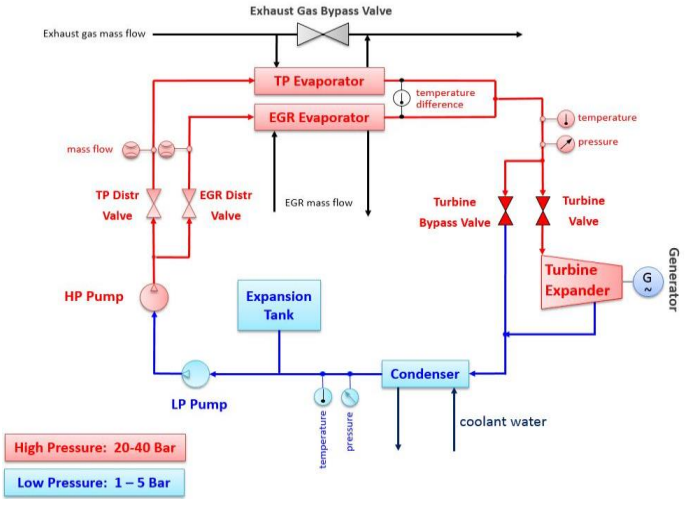

Figure 1. Schematic of ORC system for WHR

This ORC system is coupled with a 13L heavy duty diesel engine by connecting the evaporators to the tailpipe (TP) and EGR circuits. A TP evaporator bypass valve is installed in the ORC system to prevent overheating and subsequent degradation of working fluid during high load engine operation. The EGR evaporator in the ORC system replaces the stock EGR intercooler from the engine assembly. Ethanol serves as the

working fluid because of its favorable physical characteristics and environmental friendliness.

Liquid ethanol from expansion tank is pumped through the parallel evaporators where it undergoes evaporation by absorbing heat from engine exhaust gas. Ethanol vapor from both evaporators is mixed before passing through a turbine expander to generate mechanical power that drives electrical generator. Finally, after passing through the turbine, the ethanol vapor is condensed back to liquid state in the condenser. A turbine inlet valve and a turbine bypass valve work together to ensure safe turbine expander operation away from the two phase dome and smooth start/stop. The turbine bypass valve also regulates the evaporator outlet pressure.

III. ORC SYSTEM MODELING

To facilitate the control design, a physics based model is developed for the key ORC system components. In this regard, the heat transfer between working fluid and exhaust gas inside the evaporator is modeled based on conservation of mass and energy balance. The heat exchanger model assumes helical coil construction where the flow between hot gas and working fluid is separated by wall. As a result, the energy balance is considered in three separate media: working fluid, wall and exhaust gas. In addition, mass balance is considered for working fluid only to simulate the flow rate as ethanol undergoes the phase change phenomenon. To simplify the heat exchanger model, the following two assumptions are made: 1) the heat conduction in axial direction of the evaporator is neglected for all media (working fluid, exhaust gas and wall); 2) vapor inside heat exchanger is assumed to be incompressible. For an extended discussion and other modeling considerations, one can refer to [7]. The following coupled, 1-D partial differential equations (PDE) along the working fluid flow direction (z-axis) summarize the evaporator model:

$$A_f \frac{\partial \rho_f}{\partial t} + \frac{\partial \dot{m}_f}{\partial z} = 0 \tag{1a}$$

$$\rho_f V_f \frac{\partial h_f}{\partial t} = -\dot{m}_f L \frac{\partial h_f}{\partial z} + A_f U_f (T_w - T_f) \tag{1b}$$

$$\rho_g C_{pg} V_g \frac{\partial T_g}{\partial t} = \dot{m}_g C_{pg} L \frac{\partial T_g}{\partial z} + A_g U_g (T_w - T_g) \tag{1c}$$

$$\rho_w C_{pw} V_w \frac{\partial T_w}{\partial t} = -A_f U_f (T_w - T_f) - A_g U_g (T_w - T_g) \tag{1d}$$

where ρ, c_p and V are the density, specific heat capacity and volume occupied by a given media, respectively; T is temperature; h is enthalpy; A is area; $\dot{m}$ is mass flow rate; and U is heat transfer coefficient. The subscripts f, g and w represent working fluid, exhaust gas and wall, respectively; L is the heat exchanger total length.

For the exhaust gas energy balance in (1c), a change is made from [7] . For numerical tractability, the exhaust gas enthalpy is approximated by $h_g = C_{pg} T_g$. The density and specific heat capacity of exhaust gas are considered constant while working fluid density changes as a function enthalpy. Pressure dynamics are derived from modeling the compressible working fluid vapor in the pipes between the evaporators, the turbine inlet valve and the turbine bypass valve. The same conservation principles are applied to this compressible vapor volume. In this study, we limit the ORC component modeling discussion to the evaporators only. For a description of the remaining component models, as well as experimental model validation, one can consult [7].

For simulation studies, the finite volume discretization technique is used to convert the infinite dimensional problem of the coupled PDEs in (1) into a finite dimensional problem of ordinary differential equations (ODEs). Such a direct spatial PDE discretization returns large ODE systems that are not readily applicable for control and estimation purposes. For control design, we consider a 3-cell discretization using a moving boundary (MB) approach. The main idea with MB is to dynamically track the lengths of the different working fluid phases (liquid, two-phase and vapor) along the evaporator while applying the same governing differential equations in (1) to each region using control volumes [20]. A schematic of the MB models discretization is shown in Fig.2.

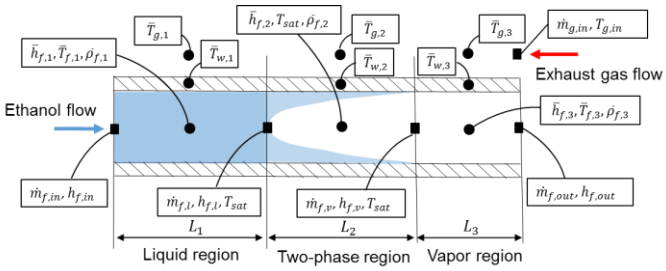

Figure 2. Moving boundary discretization schematic of the evaporator

Assuming homogenous thermodynamic properties along each control volume, lumped differential equations are derived by integrating the mass and energy conservation equations for each control volume. Following the derivation procedure detailed in [20], a sixth order ODE system is derived. Dynamics in the exhaust gas are neglected due to their fast transient characteristics. The system of differential equations are summarized below:

Liquid region:

Phase length dynamics in liquid phase (L_1):

$$\bar{\rho}_{f,1}\left(\bar{h}_{f,1} - h_{f,l}\right)\frac{dL_1}{dt} = -\frac{1}{2}AL_1\left[\bar{\rho}_{f,1} + \frac{\partial \bar{\rho}_{f,1}}{\partial h}\left(\bar{h}_{f,1} - h_{f,l}\right)\right]\frac{dh_{in}}{dt} + \dot{m}_{f,in}\left(h_{f,in} - h_{f,l}\right) + \pi d_{tube} L_1 U_{fw,1}\left(\bar{T}_{w,1} - \bar{T}_{f,1}\right) \tag{2a}$$

Wall temperature dynamics ($\bar{T}_{w,1}$):

$$Ac_p \rho_w L_1 \frac{d\bar{T}_{w,1}}{dt} + Ac_p \rho_w \left(\bar{T}_{w,1} - \bar{T}_{w,l}\right)\frac{dL_1}{dt} = \pi d_{tube} L_1 U_{fw,1}\left(\bar{T}_{f,1} - \bar{T}_{w,1}\right) + \eta \pi d_{shelleqv} L_1 m_{HTC} U_{g,w}\left(\bar{T}_{TP,1} - \bar{T}_{w,1}\right) \tag{2b}$$

Two-phase region:

Phase length dynamics in liquid phase (L_2):

$$A\left[\bar{\rho}_{f,1}\left(h_{fl}-h_{fg}\right)\right]\frac{dL_1}{dt}+A(1-\bar{\gamma})\left[\rho_{f,l}\left(h_{f,l}-h_{fg}\right)\right]\frac{dL_2}{dt}= -\frac{1}{2}AL_1\frac{\partial\bar{\rho}_{f,1}}{\partial h}\frac{dh_{in}}{dt}\left(h_{fl}-h_{fg}\right)+ \dot{m}_{f,in}\left(h_{f,l}-h_{f,g}\right)+ \pi d_{tube}L_2U_{fw,2}\left(\bar{T}_{w,2}-\bar{T}_{f,2}\right) \quad (3a)$$

Wall temperature dynamics ($\bar{T}_{w,2}$):

$$Ac_p\rho_wL_2\frac{d\bar{T}_{w,2}}{dt}+Ac_p\rho_w\left(\bar{T}_{w,l}-\bar{T}_{w,g}\right)\frac{dL_1}{dt}+ Ac_p\rho_w\left(\bar{T}_{w,2}-\bar{T}_{w,g}\right)\frac{dL_2}{dt}=\pi d_{tube}L_2U_{fw,1}\left(T_{sat}-\bar{T}_{w,2}\right)+ \eta\pi d_{shelleqv}L_2m_{HTC}U_{g,w}\left(\bar{T}_{TP,2}-\bar{T}_{w,2}\right) \quad (3b)$$

Vapor region:

Evaporator outlet enthalpy dynamics ($h_{f,out}$):

$$A\left[\bar{\rho}_{f,3}\left(h_{f,out}-\bar{h}_{f,3}\right)+\bar{\rho}_{f,1}\left(h_{f,g}-h_{f,out}\right)\right]\frac{dL_1}{dt}+ A\left[\bar{\rho}_{f,3}\left(h_{f,out}-\bar{h}_{f,3}\right)+\left((1-\bar{\gamma})\rho_{f,l}+\bar{\gamma}\rho_{f,g}\right)\left(h_{f,g}-h_{f,out}\right)\right]\frac{dL_2}{dt}+ \frac{1}{2}AL_3\left[\bar{\rho}_{f,3}-\frac{\partial\bar{\rho}_{f,3}}{\partial h}\left(h_{f,out}-\bar{h}_{f,3}\right)\right]\frac{dh_{f,out}}{dt}= -\frac{1}{2}AL_1\left[\frac{\partial\bar{\rho}_{f,1}}{\partial h}\left(h_{fg}-h_{f,out}\right)\right]\frac{dh_{in}}{dt}+ \dot{m}_{f,in}\left(h_{f,g}-h_{f,out}\right)+ \pi d_{tube}L_3U_{fw,3}\left(\bar{T}_{w,3}-\bar{T}_{f,3}\right) \quad (4a)$$

Wall temperature dynamics ($\bar{T}_{w,3}$):

$$Ac_p\rho_wL_3\frac{\partial\bar{T}_{w,3}}{\partial t}+Ac_p\rho_w\left(\bar{T}_{w,g}-\bar{T}_{w,3}\right)\frac{dL_1}{dt}+ Ac_p\rho_w\left(\bar{T}_{w,g}-\bar{T}_{w,3}\right)\frac{dL_2}{dt}= \pi d_{tube}L_3U_{fw,3}\left(\bar{T}_{f,3}-\bar{T}_{w,3}\right)+ \eta\pi d_{shelleqv}L_3m_{HTC}U_{g,w}\left(\bar{T}_{TP,3}-\bar{T}_{w,3}\right) \quad (4b)$$

where $L_3=L-(L_1+L_2)$, L is total length of the evaporator; d_{tube} and $d_{shelleqv}$ are the hydraulic diameters of heat exchangers on the working fluid side and exhaust gas side, respectively; m_{HTC} is a multiplier to enhance gas side heat transfer coefficient and η is a multiplier that account for heat loss between gas side and the ambient. The subscripts l and v refer to saturated liquid and saturated vapor states, respectively; the subscript $i=1,2,3$ stands for liquid, two-phase and vapor regions, respectively.

The exhaust gas temperature evolution is predicted by the following algebraic equations:

$$\bar{T}_{g,1}=\frac{\left[\pi d_{tube}L_1U_{g,w}\bar{T}_{w,1}+\dot{m}_gC_{pg}\left\{2\bar{T}_{g,2}-2\bar{T}_{g,3}+T_{g,in}\right\}\right]}{\dot{m}_gC_{pg}+\pi d_{tube}L_1U_{g,w}} \quad (5a)$$

$$\bar{T}_{g,2}=\frac{\left[\pi d_{tube}L_2U_{g,w}\bar{T}_{w,2}+\dot{m}_gC_{pg}\left\{2\bar{T}_{g,3}-T_{g,in}\right\}\right]}{\dot{m}_gC_{pg}+\pi d_{tube}L_2U_{g,w}} \quad (5b)$$

$$\bar{T}_{g,3}=\frac{\left[\pi d_{tube}L_3U_{g,w}\bar{T}_{w,3}+\dot{m}_gC_{pg}T_{g,in}\right]}{\dot{m}_gC_{pg}+\pi d_{tube}L_3U_{g,w}} \quad (5c)$$

Remark I: The moving boundary model summarized in (2-5) assumes the co-existence of all three phases of working fluid along the evaporator.

Remark II: The heat exchanger model described above can be adapted for both evaporators (TP and EGR).

For control formulation purposes, the resulting differential and algebraic equations in (2-5) can be written in the standard nonlinear state space form:

$$\begin{cases}\dot{x}=f(x,z,w,u)\\ 0=g(x,z,w)\end{cases} \quad (6)$$

where $x=\left[L_1,\bar{T}_{w,1},L_2,\bar{T}_{w,2},\bar{h}_{f,out},\bar{T}_{w,3}\right]^T$ is a state vector; $z=\left[\bar{T}_{g,1},\bar{T}_{g,2},\bar{T}_{g,3}\right]^T$ is algebraic state vector; $u=\dot{m}_{f,in}$ is a control input; $w=\left[\dot{m}_g,T_{g,in}\right]^T$ is an exogenous disturbance vector (engine input to ORC system).

IV. NONLINEAR MODEL PREDICTIVE CONTROL

In this section, the nonlinear model predictive control is formulated to regulate the mixed evaporator outlet working fluid temperature to a desired set point value. For the ORC system under consideration, the primary control input for temperature regulation is the working fluid mass flow through the pump. To split the mass flow through the parallel evaporators, two distribution valves are used as an intermediate actuation. The configuration of these control inputs including the measurable exogenous disturbance from engine is shown in Fig.3.

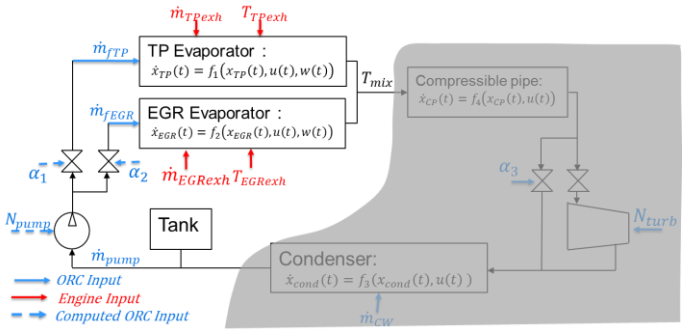

Figure 3. Control input configration for ORC system with paralel evaporators

In the following NMPC formulation, both of the mass flows ($\dot{m}_{TP}$ and $\dot{m}_{EGR}$) are considered control inputs and a nonlinear map between valve openings (α_1 and α_2) and mass flow is assumed. Similarly, pump speed can be correlated to total working fluid mass flow through the pump ($\dot{m}_{pump}=\dot{m}_{f,TP}+\dot{m}_{f,EGR}$). Two additional assumptions are made: 1) the

evaporating pressure can be controlled by a PID to a desired value in faster time response than the working fluid temperature; and 2) the condenser outlet temperature can be maintained to the desired value by adjusting coolant mass flow via an external control, such as PID.

The NMPC problem is formulated as solving a finite horizon open-loop optimal control problem subjected to system dynamics and input and state constraints on-line in repeated manner. The NMPC formulation for ORC system is given in the form:

$$\begin{aligned} &\min_{\bar{u}(\cdot)} J(x(t_i), \bar{u}(.)) \\ s.t: &\begin{cases} \dot{\bar{x}}(\tau) = f\big(\bar{x}(\tau), \bar{z}(\tau), u(\tau), w(\tau)\big), \;\; \bar{x}(t_i) = x(t_i) \\ 0 = g\big(\bar{x}(\tau), \bar{z}(\tau), w(\tau)\big), \;\; \tau \epsilon \big[t_i, t_i + T_p\big] \\ \bar{y}(\tau) = h(\bar{x}(\tau), \bar{z}(\tau), \bar{u}(\tau), w(\tau)) \end{cases} \\ &x^{lb} \le \bar{x}(\tau) \le x^{ub} \\ &y^{lb} \le \bar{x}(\tau) \le y^{ub} \\ &u^{lb} \le \bar{u}(\tau) \le u^{ub} \\ &\delta u^{lb} \le \dot{\bar{u}}(\tau) \le \delta u^{ub} \\ &\bar{u} = \big[\dot{m}_{f,TP}, \dot{m}_{f,EGR}\big]^T \end{aligned} \tag{7}$$

where J is the cost function for optimization; T_p is prediction horizon; the superscripts $lb\ and\ ub$ indicate the lower and upper bounds of the constrained variables, respectively; the bar $(\bar{\cdot})$ denotes predicted variables based on the control model using state feedback $x(t_i)$ and predicted input $\bar{u}$. Note that the control horizon is made equivalent to the prediction horizon.

The NMPC cost function is defined in a way which addresses the parallel evaporator temperature control challenge. Three variant cost functions are considered to study the relative performance of different NMPC strategies for smooth control of the mixed evaporator outlet working fluid temperature. The first natural assumption is regulating the mixed temperature by directly defining the hard constraints for safety considerations. We call this control strategy *direct control*. The second option considers regulating each of the individual evaporator outlet temperatures to the desired value independently which assumes the regulation of their mixed temperature indirectly. This is called *indirect control*. The third option controls the mixed working fluid vapor temperature directly and the temperature difference between the two evaporators. This is called *direct plus delta-T control*. These three control strategies and their corresponding cost function representations are summarized below:

1) Direct control:

$$J = \int_{t_i}^{t_i+T_p} \left\{ \frac{\left(T_d - T_{f,mix}\right)^2}{T_{max}^2} \right\} d\tau \tag{8a}$$

2) Indirect control:

$$J = \int_{t_i}^{t_i+T_p} \left\{ (I-Q) \frac{\left(T_d - T_{f,TP}\right)^2}{T_{max}^2} + Q \frac{\left(T_d - T_{f,EGR}\right)^2}{T_{max}^2} \right\} d\tau \tag{8b}$$

3) Direct plus delta-T control:

$$J = \int_{t_i}^{t_i+T_p} \left\{ (I-Q) \frac{\left(T_d - T_{f,mix}\right)^2}{T_{max}^2} + Q \frac{\left(T_{f,TP} - T_{f,EGR}\right)^2}{T_{max}^2} \right\} d\tau \tag{8c}$$

where $T_{f,mix}$ is mixed evaporator outlet temperature; T_d is desired temperature reference for control; Q is positive definite weighting matrix. The mixed temperature is calculated using thermodynamic table at a given evaporator pressure and mixed enthalpy$(p, h_{f,mix})$. The mixed enthalpy is calculated from energy balance equation given in the form:

$$\dot{m}_{pump} h_{f,mix} = \dot{m}_{f,TP} h_{f,TP} + \dot{m}_{f,EGR} h_{f,EGR} \tag{9}$$

The constraints in (7) include physical actuation limitations and safe operation of the ORC system. The actuator limitations are defined by upper and lower bounds on input values (u^{lb}, u^{ub}) as well as on the rates of input change $(\delta \dot{u}^{lb}, \delta \dot{u}^{ub})$. For safe operation, the maximum possible temperature is limited to avoid dissociation and degradation of the working fluid, which is ethanol in this study. The minimum vapor quality at the turbine inlet is set to be greater than one to avoid ethanol condensation in the turbine expander. These safety conditions are treated as output constraints (y^{lb}, y^{ub}). Considering these constraints and the above cost function, the NMPC algorithm solves for an open-loop optimal control input $\bar{u}(\cdot)$ in a repeated manner, updating the initial state conditions based on feedback information. Here, we assume the availability of full state feedback from state estimation using evaporator outlet temperature measurements.

To reduce the computational burden of the nonlinear optimization problem, a direct method of sequential quadratic programming (SQP) techniques is chosen, which considers only the control inputs as optimization variables while solving ODEs for state trajectories as a function of input using numerical integration [21]. To further reduce the number of optimization variables, the control input is parametrized by a piecewise continuous quadratic function and the optimization is carried out in the parameter space. For forward prediction of state trajectories, an implicit numerical integration method called the Rosenbrock-Wanner (ROW) method was used. The ROW method compromises between the disadvantages of both explicit and implicit Runge-Kutta methods, making it suitable for a stiff-ODE system. The ORC system happens to be a stiff-ODE due to the very small mass of working fluid in the vapor regions. For ORC system dynamics in (7), 2-stage ROW method is summarized as follows:

$$\begin{aligned} x_{n+1} &= x_n + dt \sum_{i=1}^{2} b_i k_i \\ W_n k_i &= f\left(x_n + dt \sum_{i=1}^{i-1} a_{ij} k_j \right) + dt J_n \sum_{i=1}^{i-1} d_{ij} k_j \,, \; i \\ &= 1,2 \\ W_n &= I - dt d_{ii} J_n, \;\; J_n = \frac{\partial f(x_n)}{\partial x} \end{aligned} \tag{10}$$

The coefficients for 2nd-stage ROW method are: $a_{21} = \frac{2}{3}, d_{11} = 1 + \frac{1}{\sqrt{2}}, d_{21} = -\frac{4}{3}, b_1 = \frac{1}{4}$ & $b_2 = 3/4$. For detail derivation of the ROM method, one can refer [22]. With the ROW integration method, a larger time step can be used for forward prediction, and the NMPC computation burden is reduced.

V. RESULTS AND DISCUSSIONS

In this section, simulation results are presented to demonstrate the NMPC controller performance. The simulated plant model is the coupled PDE form of (1), where 30 cell-based discretization is used to convert the PDEs to system of ODEs via finite volume discretization techniques. The reduced order moving boundary model summarized in (2-5) is then utilized for the NMPC optimization. Two engine operating points of varying load are considered in the simulations to demonstrate the NMPC performance. The selected engine operating points are summarized in Table 1.

The simulation results are presented in three parts. First, the performance of the three aforementioned control strategies is compared in (Figs.4-5) while applying the NMPC to the same control model. Second, the NMPC performance over the experimentally validated plant model (Finite Volume Method) considering a step change in mixed vapor temperature set point is presented. The third part of the simulation results (Figs.7-8) compares the performance of NMPC and PID control for the two engine operating points. Note that, for all simulation cases, the ORC system is initialized in warm conditions, namely, all three phases of working fluid are present in the moving boundary model.

Table 1: Selected engine operating points for simulation

Case	Evap.	Speed (rpm)	Torque (Nm)	EGR rate (%)	$\dot{m}_g$ (kg/s)	$T_{g,in}$ (K)
1	TP	1575	1540	12	0.337	686
	EGR				0.044	807
2	TP	1300	700	12	0.156	625
	EGR				0.023	654

Figure 4 shows the mixed working fluid vapor temperature control achieved by all three control strategies. In all cases, the mixed temperature tracks the set point value smoothly. However, undesirable response is observed for the EGR evaporator outlet temperature when using the direct control strategy (Fig. 4a). This errant behavior could potentially exceed the vapor temperature boundaries established for system safety in either evaporators although the control maintains the desired mixed temperature. The other two control cases, Direct+Delta-T control and Indirect Control, exhibit very smooth control response for both the TP and EGR evaporator exit temperatures as a result of the extra penalty term included in the NMPC formulation, establishing a coordinated control effort.

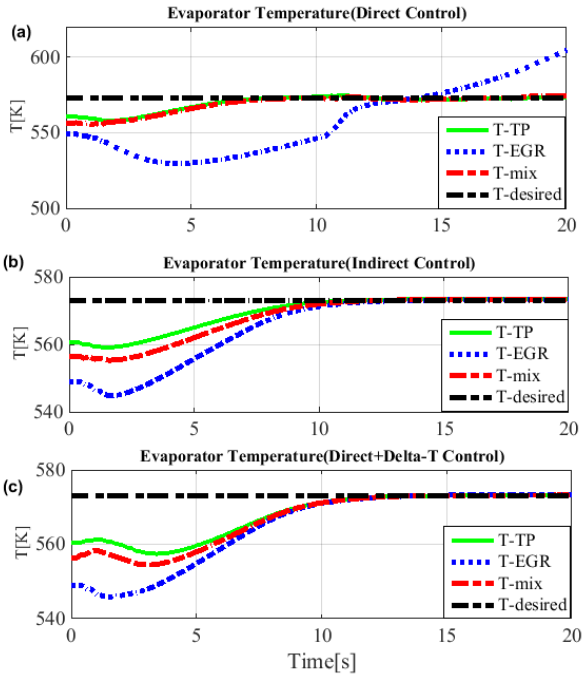

Figure 4: Temperature control response by different NMPC control strategies for the Case 1 engine operating condition: a) direct plus delta-T control, b) indirect control, and c) direct control

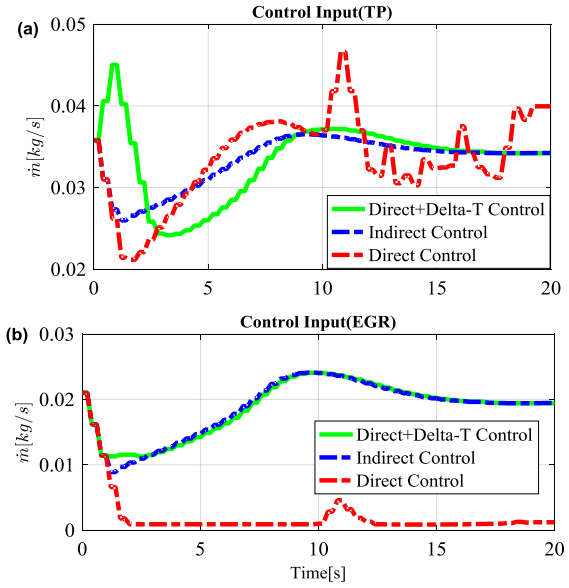

Figure 5: Control input of working fluid mass flow for all three control strategies for the Case 1 engine operating condition: a) mass flow through TP, and b) mass flow through EGR

The effect of the penalty term for coordinated control is obvious from the control input plot in Fig. 5. For direct control case, which includes no cost for coordinated control, the working fluid mass flow through the TP evaporator experiences multiple oscillations while the flow through the EGR evaporator stays constant for a prolonged duration. In other two control strategies, which include the additional cost term, the split of working fluid

mass flow through the TP and EGR evaporators is proportional and smooth. For the simulation of engine operating condition 'Case 1', a comparative control response is achieved by 'indirect control' and 'direct plus delta-T' control. However, the indirect control strategy may fail in cases where insufficient hot gas passes through one of the evaporators because the indirect control forces the control of the evaporator exit temperatures independent of the mixed vapor temperature set point. Therefore, 'direct plus delta-T' control is utilized for the following sections.

Figure 6 examines the direct plus delta-T control during a stepped set point temperature demand. The corresponding control input is achieved by a reduced order model based NMPC applied over the full physics based plant model. The aggressive mixed vapor temperature set-point changes are controlled by the NMPC in a very short control response time of about 10 seconds. As a result of the additional NMPC cost function penalty term, a coordinated actuation effort is observed in both evaporator mass flow rates in proportion to exhaust energy input to the respective evaporators.

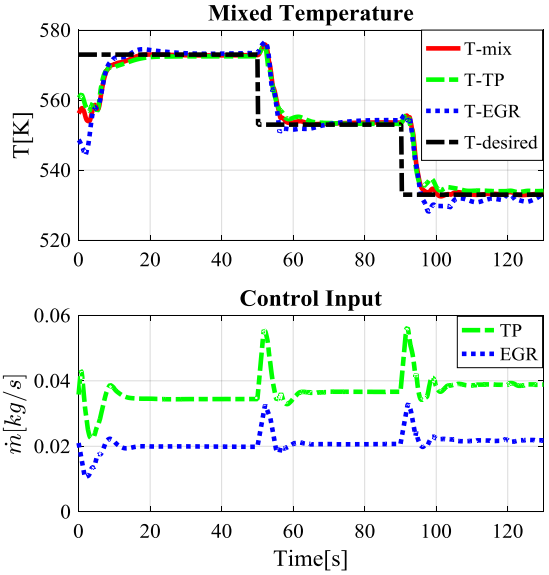

Figure 6: Stepped temperature control response and corresponding control input determined by the NMPC for the Case 1 engine operating condition

In figures 7 and 8, the performance of NMPC and PID controllers are compared for a stepped mixed vapor temperature set point command. For Case 1 engine conditions (Fig.7), the NMPC tracks the desired temperature step change smoothly with a time response of about 10seconds while PID continues to oscillate around set point temperature. For Case 2 engine conditions (Fig.8), the NMPC achieved smooth control response with a time response of about 20 seconds while the PID took over 60 seconds for convergence and experienced a very large overshoot in the EGR evaporator temperature, which could potentially violate the vapor temperature boundary constraints. Note that the PID control gains are tuned for the same control strategies as the NMPC (direct control plus delta-T control).

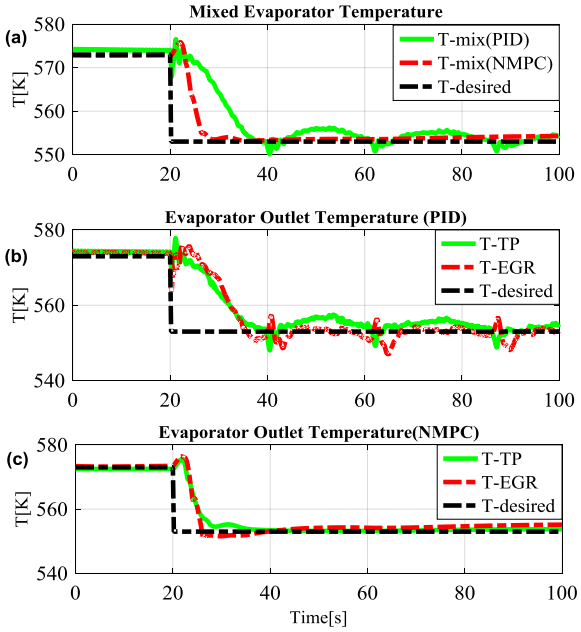

Figure 7: Stepped temperature control response by NMPC and PID control for the Case 1 engine operating conditions

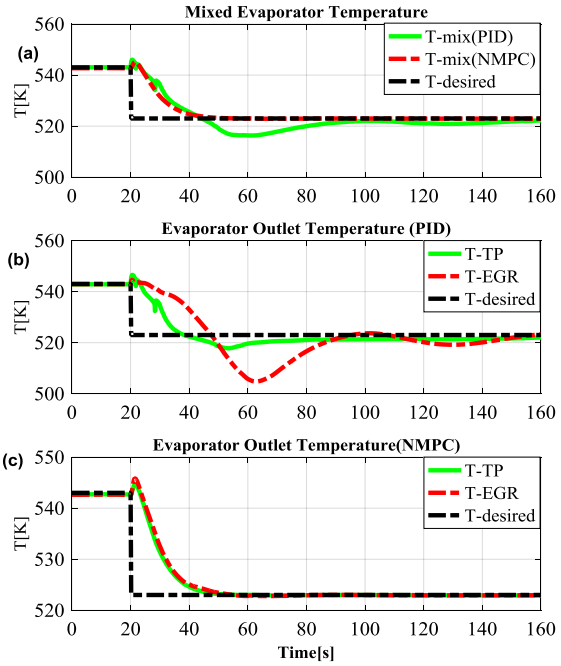

Figure 8: Stepped temperature control response by NMPC and PID control for the Case 2 engine operating conditions

The simulation studies discussed in this section demonstrated a superior performance of NMPC over a classical PID control. However, the real time implementation of NMPC depends on the efficiency of the solver used for the optimization. The optimization algorithm of the solver used in this study is implemented in Matlab and doesn't precisely meet the time constraint for online implementation. The efficiency of the solver could be improved if it is implemented in an efficient

program language environment such as C and C++. An efficient C++ code can also auto-generated using available commercial software such as ACADO[23]. In this study, we like to limit the discussion to theoretical merit of NMPC while continue to research on the real-time implementation challenge in the future studies.

VI. CONCLUSIONS

In this paper, a NMPC scheme is proposed for mixed vapor temperature control of a parallel evaporator ORC system for heavy duty engine waste heat recovery. The NMPC is designed based on a reduced order control-oriented moving boundary heat exchanger model. For a smooth control response of the ORC system utilizing parallel evaporators, a penalty cost function term on temperature difference is added in the NMPC formulation, accounting for the coordinated actuation of both evaporator mass flow rates from single input source of total working fluid mass flow. To address the numerical challenges related to ORC system dynamic stiffness, an implicit numerical integration method was adopted that can use a larger time step for forward prediction, reducing the NMPC computation burden.

Benefits of the proposed NMPC were demonstrated through simulations studies that consider an aggressive step change of set point temperature while applying the control input over an experimentally validated, high fidelity, physics-based ORC plant model. Three control strategies were compared and the coordinated control 'direct control plus delta-T' proved the best response of mixed vapor temperature while minimizing the possibility for either individual evaporator exit temperature to violate operational boundaries.

The NMPC was also compared with PID control tuned for the same 'direct plus delta-T' control strategy at two sets of engine operating conditions. The NMPC exhibited enhanced performance in-terms of minimum control response time, minimum overshoot, and precise regulation of mixed evaporator temperature.

Future work includes NMPC performance evaluation under varying engine conditions and real-time implementation of the NMPC algorithm on an embedded platform.

REFERENCES

[1] EPA, "EPA and NHTSA adopt first-ever program to reduce greenhouse gas emissions and improve fuel efficiency of medium- and heavy-duty vehicles," 2011.

[2] O. Delgado and N. Lutsey, "The U.S SuperTruck Program: Expediting the Development of Advanced Heavy-Duty Vehicle Efficiency Technologies," The International Council on Clean Transportation2014.

[3] T. Park, H. Teng, G. L. Hunter, B. van der Velde, and J. Klaver, "A Rankine Cycle System for Recovering Waste Heat from HD Diesel Engines - Experimental Results," SAE International, Warrendale, PA 2011-01-1337, 2011.

[4] H. Teng, G. Regner, and C. Cowland, "Achieving High Engine Efficiency for Heavy-Duty Diesel Engines by Waste Heat Recovery Using Supercritical Organic-Fluid Rankine Cycle," SAE International, Warrendale, PA 2006-01-3522, 2006.

[5] H. Teng and G. Regner, "Improving Fuel Economy for HD Diesel Engines with WHR Rankine Cycle Driven by EGR Cooler Heat Rejection," SAE International, Warrendale, PA 2009-01-2913, 2009.

[6] H. Teng, G. Regner, and C. Cowland, "Waste Heat Recovery of Heavy-Duty Diesel Engines by Organic Rankine Cycle Part II: Working Fluids for WHR-ORC," SAE International, Warrendale, PA, SAE Technical Paper 2007-01-0543, 2007.

[7] B. Xu, X. Liu, J. Shutty, P. Anschel, S. Onori, Z. Filipi, *et al.*, "Physics-Based Modeling and Transient Validation of an Organic Rankine Cycle Waste Heat Recovery System for Heavy-Duty Diesel Engine Applications," presented at the SAE International, Detroit, 2016.

[8] D. Seher, T. Lengenfelder, G. Jurgen, E. Nadja, H. Michael, and I. Krinn, "Waste Heat Recovery for Commercial Vehicles with a Rankine Process," *21st Aachen Colloquium Automobile and Engine technology*, 2012.

[9] B.-R. Fu, S.-W. Hsu, C.-H. Liu, and Y.-C. Liu, "Statistical analysis of patent data relating to the organic Rankine cycle," *Renewable and Sustainable Energy Reviews*, vol. 39, pp. 986-994, 2014.

[10] F. Vélez, J. J. Segovia, M. C. Martín, G. Antolín, F. Chejne, and A. Quijano, "A technical, economical and market review of organic Rankine cycles for the conversion of low-grade heat for power generation," *Renewable and Sustainable Energy Reviews*, vol. 16, pp. 4175-4189, 2012.

[11] H. Chen, D. Y. Goswami, and E. K. Stefanakos, "A review of thermodynamic cycles and working fluids for the conversion of low-grade heat," *Renewable and Sustainable Energy Reviews*, vol. 14, pp. 3059-3067, 2010.

[12] T. C. Hung, T. Y. Shai, and S. K. Wang, "A review of organic rankine cycles (ORCs) for the recovery of low-grade waste heat," *Energy*, vol. 22, pp. 661-667, 1997.

[13] M. C. Esposito, N. Pompini, A. Gambarotta, V. Chandrasekaran, J. Zhou, and M. Canova, "Nonlinear Model Predictive Control of an Organic Rankine Cycle for Exhaust Waste Heat Recovery in Automotive Engines," *IFAC-PapersOnLine*, vol. 48, pp. 411-418, 2015.

[14] D. Luong and T. C. Tsao, "Linear Quadratic Integral Control of an Organic Rankine Cycle for Waste Heat Recovery in Heavy-Duty Diesel Powertrain," *2014 American Control Conference (Acc)*, pp. 3147-3152, 2014.

[15] E. Feru, F. Willems, B. de Jager, and M. Steinbuch, "Model predictive control of a waste heat recovery system for automotive diesel engines," in *System Theory, Control and Computing (ICSTCC), 2014 18th International Conference*, 2014, pp. 658-663.

[16] J. H. Zhang, Y. L. Zhou, S. Gao, and G. L. Hou, "Constrained Predictive Control Based on State Space Model of Organic Rankine Cycle System for Waste Heat Recovery," *Proceedings of the 2012 24th Chinese Control and Decision Conference (Ccdc)*, pp. 230-234, 2012.

[17] J. Peralez, P. Tona, A. Sciarretta, P. Dufour, and M. Nadri, "Towards model-based control of a steam Rankine process for engine waste heat recovery," in *2012 IEEE Vehicle Power and Propulsion Conference (VPPC)*, 2012, pp. 289-294.

[18] J. Peralez, P. Tona, O. Lepreux, A. Sciarretta, L. Voise, P. Dufour, *et al.*, "Improving the Control Performance of an Organic Rankine Cycle System for Waste Heat Recovery from a Heavy-Duty Diesel Engine using a Model-Based Approach," *2013 Ieee 52nd Annual Conference on Decision and Control (Cdc)*, pp. 6830-6836, 2013.

[19] A. Hernandez, A. Desideri, C. Ionescu, S. Quoilin, V. Lemort, and R. D. Keyser, "Increasing the efficiency of Organic Rankine Cycle Technology by means of Multivariable Predictive Control," in *In Proceedings of the 19th World Congress of the International Federation of Automatic Control (IFAC 2014)*, 2014.

[20] J. M. Jensen, "Dynamic Modeling of Thermo-Fluid Systems with Focus on Evaporators for Refrigeration," Energy Engineering, Department of Mechanical Engineering, Technical University of Denmark, 2003.

[21] B. Chachuat, " Nonlinear and Dynamic Optimization: From Theory to Practice", Automatic Control Laboratory, 2007|.

[22] H. Zedan, "An an-Stable Rosenbrock-Type Method for Solving Stiff Differential-Equations," *Computers & Mathematics with Applications*, vol. 13, pp. 611-615, 1987.

[23] B. Houska and H.J. Ferreau and M. Diehl, "ACADO Toolkit--An Open Source Framework for Automatic Control and Dynamic Optimization," *Optimal Control Applications and Methods*, vol. 32, iss. 3, pp. 298-312, 2011.